Narrow-Linewidth Homogeneous Optical Emitters in Diamond Nanostructures via Silicon Ion Implantation

Ruffin E. Evans,[1] Alp Sipahigil,[1] Denis D. Sukachev,[1,2] Alexander S. Zibrov,[1] and Mikhail D. Lukin[1,*]

[1]*Department of Physics, Harvard University, 17 Oxford Street, Cambridge, Massachusetts 02138, USA*
[2]*Russian Quantum Center, Business-center "Ural," 100A Novaya Street, Skolkovo, Moscow 143025, Russia*
(Received 15 December 2015; revised manuscript received 15 March 2016; published 18 April 2016)

The negatively charged silicon-vacancy (SiV^-) center in diamond is a bright source of indistinguishable single photons and a useful resource in quantum-information protocols. Until now, SiV^- centers with narrow optical linewidths and small inhomogeneous distributions of SiV^- transition frequencies have only been reported in samples doped with silicon during diamond growth. We present a technique for producing implanted SiV^- centers with nearly lifetime-limited optical linewidths and a small inhomogeneous distribution. These properties persist after nanofabrication, paving the way for the incorporation of high-quality SiV^- centers into nanophotonic devices.

DOI: 10.1103/PhysRevApplied.5.044010

I. INTRODUCTION

Coherent emitters of indistinguishable single photons are a basic ingredient in many quantum-information systems [1]. Atomlike emitters in the solid state are a particularly appealing platform for practical quantum information because they can be scalably integrated into nanophotonic devices. However, no single solid-state system has yet combined high brightness of narrow-band emission and a low inhomogeneous distribution of photon frequencies from separate emitters (indistinguishability) with ease of incorporation into nanophotonic structures on demand. For example, optically active semiconductor quantum dots can be bright and integrable into nanostructures, but have a large inhomogeneous distribution [2]. Nitrogen-vacancy (NV^-) centers in bulk diamond [3] are bright and photostable, with a moderate inhomogeneous distribution that allows the straightforward tuning of multiple NV^- centers into resonance. These properties allow proof-of-principle demonstrations of quantum-information protocols such as remote spin-spin entanglement generation [4,5] and quantum teleportation [6]. Further progress towards developing NV^--based quantum devices has been hindered by low indistinguishable photon-generation rates associated with the weak NV^- zero-phonon line (ZPL), a challenge that could be addressed by integrating NV^- centers into nanophotonic structures. However, the optical transition frequencies of NV^- centers are very sensitive to their local environment [7,8], making integration of spectrally stable emitters into nanophotonic structures a major challenge [9].

The negatively charged silicon-vacancy color center in diamond (SiV^-) has shown promise in fulfilling the key criteria of high brightness [10], lifetime-limited optical linewidths [11], and a narrow inhomogeneous distribution of optical transition frequencies [12]. The SiV^- (Fig. 1) has electronic states with strong dipole transitions where 70% of the emission is in the ZPL at 737 nm [10]. The inversion symmetry of the SiV^- prevents first-order Stark shifts, suppressing spectral diffusion [11] and allowing indistinguishable photons to be generated from separate emitters without the need for tuning or extensive preselection of emitters [14]. When combined with a spin degree of freedom [15], the SiV^- center's bright narrow-band transition, narrow inhomogeneous distribution, and spectral stability make it a promising candidate for applications in quantum optics and quantum information science.

Silicon-vacancy centers occur only rarely in natural diamond [16], and are typically introduced during CVD growth via deliberate doping with silane [17,18] or via silicon contamination [11,12,19–21]. While these techniques typically result in a narrow inhomogeneous distribution of SiV^- fluorescence wavelengths, these samples have a number of disadvantages. For example, the concentration of SiV^- centers can be difficult to control and localization of SiV^- centers in three dimensions is impossible.

Ion implantation offers a promising solution to these problems. By controlling the energy, quantity, and isotopic purity of the source ions, the depth, concentration, and isotope of the resulting implanted ions can be controlled. Ion implantation is widely commercially available. Targeted ion implantation using a focused silicon ion beam is also possible, allowing for the placement of silicon defects in all three dimensions with precision on the scale of tens of nanometers [22]. Despite the advantages of ion implantation, there have been conflicting results [13,22,23] on the brightness and creation yield of SiV^- centers produced using this method and no systematic studies of the inhomogeneous distribution of SiV^- fluorescence

[*]lukin@physics.harvard.edu

 © 2016 American Physical Society

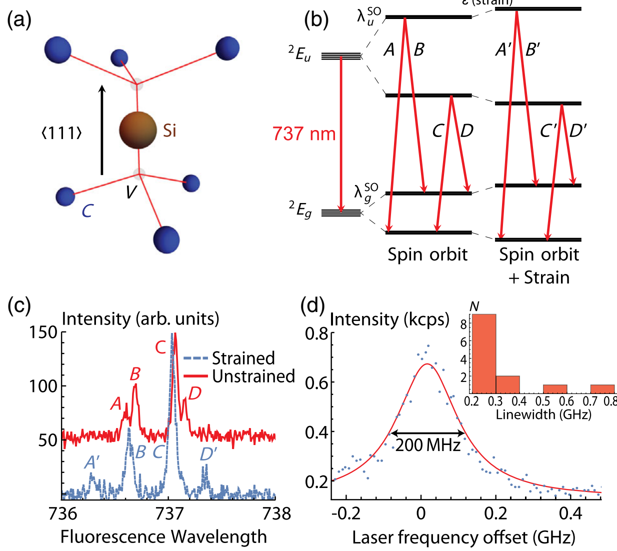

FIG. 1. Properties of the SiV$^-$ center. (a) Atomic structure of the SiV center. The V-Si-V axis lies along the ⟨111⟩ lattice direction. The SiV$^-$ has D_{3d} symmetry. (b) Level structure of the SiV$^-$ center. The SiV$^-$ is a single-hole system with double orbital and spin degeneracy. This degeneracy is partially lifted by spin-orbit coupling ($\lambda_g^{SO} = 47$ GHz and $\lambda_u^{SO} = 260$ GHz [11,13]). Lattice strain increases the splitting between these spin-orbit levels, shifting the transition frequencies. (c) Fluorescence spectra of the ZPLs of single SiV$^-$ centers in high-strain (blue, dashed) and low-strain (red) environments at 9–15 K. Transitions B and C are less sensitive to strain compared with transitions A and D because the ground and excited states shift in the same (opposite) directions for transitions B and C (A and D) [12]. Unstrained spectrum offset and scaled vertically for clarity. (d) Linewidth (FWHM) of representative implanted SiV$^-$ in bulk (unstructured) diamond measured by PLE spectroscopy (blue points, data; red line, Lorentzian fit). Inset: histogram of emitter linewidths in bulk diamond. Almost all emitters have a linewidth within a factor of 3 of the lifetime limit (94 MHz).

wavelengths. Although there has been a single report of an implanted SiV$^-$ with a linewidth roughly 10 times the lifetime limit [24], to the best of our knowledge there has been no consistent method for producing SiV$^-$ centers with bright, narrow-linewidth emission using ion implantation. These two criteria of a low inhomogeneous distribution relative to the single-emitter linewidth and narrow single-emitter linewidth relative to the lifetime limit are essential for quantum-optics applications [1,25].

In this paper, we report the creation of SiV$^-$ centers in diamond using ion implantation. Implantation is followed by high-temperature high-vacuum annealing to facilitate SiV$^-$ formation and repair implantation-induced damage to the lattice. The resulting emitters have narrow optical transitions within a factor of 4 of the lifetime-limited linewidth and a narrow inhomogeneous distribution such that half of the emitters have transitions that lie in a 15-GHz window. Finally, we incorporate these SiV$^-$ centers into nanostructures and demonstrate that their favorable optical properties are maintained even after fabrication.

II. THE SiV$^-$ CENTER IN DIAMOND

The silicon-vacancy color center is a point defect in diamond wherein a silicon atom occupies an interstitial position between two vacancies [Fig. 1(a)] [26]. The SiV$^-$ is a spin-$\frac{1}{2}$ system with ground (^2E_g) and excited (^2E_u) states localized to the diamond band gap [26–28]. Both states have double spin and orbital degeneracies partially lifted by the spin-orbit interaction [Fig. 1(b)] which splits each quartet into two degenerate doublets. The spin-orbit splittings for the ground and excited states are 0.19 and 1.08 meV (47 and 260 GHz), respectively [Fig. 1(c)] [13,27]. All transitions between the ground and excited states are dipole allowed with a ZPL energy of 1.68 eV ($\lambda = 737$ nm) and an excited-state lifetime of under 1.7 ns [29]. These optical transitions can have linewidths [Fig. 1(d)] comparable to the lifetime limit of 94 MHz [11].

The SiV$^-$ is sensitive to strain, which can both shift the average energy (for axial strain) and increase the splitting (for transverse strain) in the ground and excited-state manifolds [Fig. 1(b), last column] [13,15]. Transitions B and C within the ZPL are relatively insensitive to transverse strain because their ground and excited states shift in the same direction: both upward for transition B and both downward for transition C [Fig. 1(c)] [12]. Transition C is between the lowest-energy ground and excited states which are also isolated from the phonon bath at low temperatures [29]. This transition is therefore the most suitable for applications in quantum information science.

III. CREATING SiV$^-$ CENTERS WITH ION IMPLANTATION

We create SiV$^-$ centers using the following procedure: First, we begin with a polished CVD diamond (Element Six Inc., $[N]_S^0 < 5$ ppb, {100} oriented top face). Previous work suggests that mechanical polishing produces a strained and damaged layer close to the surface that results in reduced mechanical stability of nanofabricated structures [30]. We also expect that the strain introduced by mechanical polishing will lead to a larger inhomogeneous distribution of SiV$^-$ wavelengths. We reduce this damage by removing 5 μm of diamond through reactive ion etching, producing a smooth (under 1-nm rms roughness) surface. More details on this technique can be found elsewhere [30,31]. An otherwise identical control sample is also put through the same implantation procedure but without this pre-etching step. We then implant $^{29}Si^+$ ions (Innovion Corporation) at a dose of 10^{10} ions/cm^2 and an energy of 150 keV resulting in an estimated depth of 100 ± 20 nm [32].

After implantation, we clean the samples using an oxidative acid clean (boiling 1:1:1 perchloric:nitric:sulfuric

acid) [33] and then perform two high-temperature high-vacuum ($\lesssim 10^{-6}$ Torr) anneals. The first anneal is at 800 °C for eight hours after a four-hour bakeout step at 400 °C. At 800 °C, vacancies are mobile [34–36] leading to the formation of SiV^- centers. The second anneal is the same as the first, but with an additional step at 1100 °C with a two-hour dwell time. At this temperature, divacancies and other defects can also anneal out [37,38]. For all annealing steps, we use slow temperature ramps ($\lesssim$35 °C per hour) to maintain low pressures in our furnace. This annealing procedure, inspired by previous work with SiV^- [20,39] and NV^- [31,37,40,41] centers, both aids in the formation of SiV^- centers and also helps remove damage to the crystal lattice, reducing local strain. The residual graphitic carbon produced during these high-temperature anneals is removed by again performing the oxidative acid clean. Before each annealing step, we use x-ray photoelectron spectroscopy to verify that the surface is free of contaminants.

IV. RESULTS AND DISCUSSION

A. SiV^- centers in bulk diamond

We confirm that the SiV^- centers exhibit narrow-linewidth optical transitions by performing photoluminescence excitation (PLE) spectroscopy after 1100 °C annealing. In this experiment, we scan the frequency of a weak resonant laser (New Focus Velocity, linewidth $\Delta f \lesssim$ 25 MHz over the course of the experiment, stabilized with a High Finesse WS7 wave meter) across transition C and monitor the fluorescence on the phonon sideband (PSB). We integrate over several scans to reconstruct the time-averaged shape and position of the SiV^- ZPL [Fig. 1(d)]. We perform these measurements in a helium-flow cryostat at a sample stage temperature of 3.7 K to avoid phonon-induced broadening of the optical transition [29]. The emitters are resonantly excited below saturation to avoid power broadening. (See Appendix A for more experimental details.) We find that SiV^- centers in bulk diamond have narrow optical transitions with linewidths of $\Gamma/2\pi = 320 \pm 180$ MHz (mean and standard deviation for $N = 13$ spatially resolved emitters). Almost all SiV^- centers have a linewidth within a factor of 3 of the lifetime limit [Fig. 1(d), inset]. As defined here, these linewidths include the effects of phonon broadening and all spectral diffusion that happens at any time scale during the course of the experiment (4–15 minutes).

We characterize the inhomogeneous distribution of the implanted SiV^- fluorescence wavelengths after each annealing step via photoluminescence spectroscopy. To perform these measurements, we excite the SiV^- centers using off-resonant light from a 700-nm diode laser. Off-resonant excitation at 520 nm is also possible. Using both of these wavelengths together results in a superlinear enhancement in the observed count rate, suggesting that the 520-nm laser may play a role in stabilizing the SiV^- charge state. The resulting fluorescence is sent to a spectrometer (Horiba iHR550, 0.025-nm resolution). We perform these measurements at 9–15 K.

After annealing at 800 °C, the observed distribution is broad, with about half of the emitter transition wavelengths lying within a (3–4)-nm range [Fig. 2(a), red dashed curve]. Transition C is used where unambiguous identification is possible; otherwise, the brightest transition (which should correspond to transition C [11,12]) is used. After the 1100 °C anneal, the distribution becomes more than 100

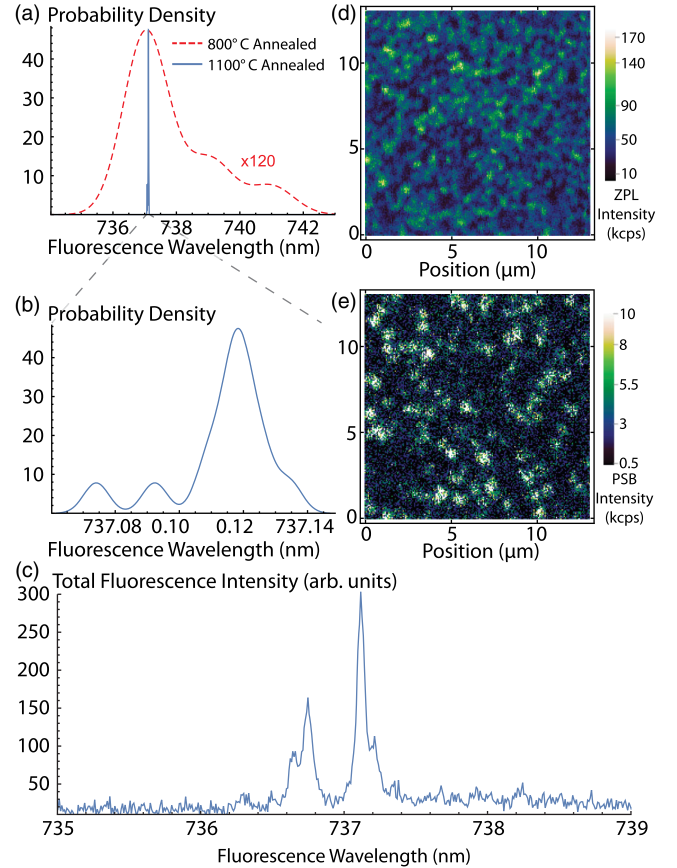

FIG. 2. Inhomogeneous distribution of fluorescence wavelengths of implanted SiV^- transitions. (a) Kernel density estimation of distribution of bulk SiV^- wavelengths after 800 °C ($N = 19$, red dashed curve) and 1100 °C ($N = 13$, blue solid curve) annealing. The distribution narrows from 3–4 nm (800 °C anneal) to 0.03 nm (15 GHz, 1100 °C anneal). (b) Enlarged distribution (transition C) after 1100 °C annealing. Note the smaller wavelength range on the horizontal axis. (c) Sum of spectra for different SiV^- centers after 1100 °C annealing. The SiV^- fine structure is clearly present, demonstrating that the inhomogeneous distribution is small. (d),(e) Spatial map of collected fluorescence (thousands of counts per second) over a region of bulk diamond exciting off (d) and on (e) resonance. By comparing the densities of emitters, we estimate that $(30 \pm 15)\%$ of the emitters are nearly resonant. These measurements are taken at 9–15 K.

times narrower, with about half of the 13 measured emitters (transition C) now lying in a 0.03-nm (15-GHz) window [Figs. 2(a) and 2(b), blue solid curves]. In both cases, we focus on transition C because it is the brightest transition and relatively insensitive to strain [12] and phononic decoherence [29]. The other transitions are also much more narrowly distributed after 1100 °C annealing. In Fig. 2(c), we plot a composite spectrum constructed by summing over all of the normalized 13-SiV^- spectra taken after 1100 °C annealing. This composite spectrum is very similar to the spectrum of a single unstrained SiV^- center [Fig. 1(c)] and shows the expected fine-structure splitting, demonstrating that the inhomogeneous distribution of SiV^- transition wavelengths is small compared to the fine-structure splitting. This result is comparable to reported inhomogeneous distributions reported for SiV^- centers created during CVD growth [11–14]. It is possible that even higher-temperature annealing could further reduce this inhomogeneous distribution [20,41].

To estimate the yield of conversion from implanted Si^+ ions to SiV^- centers, we perform scanning confocal microscopy [Fig. 2(d)]. Exciting with several milliwatts of off-resonant light (700 nm) gives around 10^5 counts per second (cps) into a single-mode fiber from a single SiV^- in a 20-nm spectral range around the ZPL. In the resulting microscope image, we count the number of SiV^- centers and estimate a density of $0.5–1/\mu m^2$. Based on our Si^+ implantation density of $100/\mu m^2$, we estimate our SiV^- creation yield after 800 °C annealing to be (0.5–1)%. There is no clear difference in the yield after performing the 1100 °C anneal. Furthermore, the yield in the sample that is not pre-etched is significantly higher [(2–3)%]. The observations that higher-temperature annealing did not increase the yield and that the sample with greater surface damage had a larger yield both support the model that SiV^- formation is limited by the presence and diffusion of nearby vacancies [38,39]. This yield could be increased by electron irradiating the sample to create a higher vacancy density in a controllable way [18,37,39].

To visualize the density of nearly resonant SiV^- centers, we resonantly excited the SiV^- centers with a Rabi frequency of several GHz using an external-cavity diode laser tuned to the center of the inhomogeneous distribution. We scan spatially over the sample and collect fluorescence on the PSB. The resulting image taken in the same region of the sample [Fig. 2(e)] has about a factor of 3 fewer emitters compared to the image taken with off-resonant excitation ($N \sim 100$ vs ~ 340); roughly 30% of the emitters are near resonant (within our few-GHz Rabi frequency).

B. SiV^- centers in nanostructures

One major advantage of building quantum devices with solid-state emitters rather than trapped atoms or ions is that solid-state systems are typically more easily integrated into nanofabricated electrical and optical structures [42,43]. The scalability of these systems is important for the practical realization of even simple quantum optical devices [44]. Unfortunately, many solid-state systems suffer serious deterioration in their properties when incorporated into nanostructures. For example, the large permanent electric dipole of NV^- centers in diamond causes coupling of the NV^- to nearby electric field noise, shifting its optical transition frequency as a function of time. The SiV^- is immune to this spectral diffusion to first order because of its inversion symmetry [14] and is therefore an ideal candidate for integration into diamond nanophotonic structures. Motivated by these considerations, we fabricated an array of diamond nanophotonic waveguides [Fig. 3(a)] on the pre-etched sample characterized above using previously reported methods [30,45]. Each waveguide [Fig. 3(a), inset] is 23-μm long with approximately equilateral-triangle cross sections of side length 300–500 nm. After fabrication, we again perform the same 1100 °C annealing and acid cleaning procedure. Many SiV^- centers are visible in a

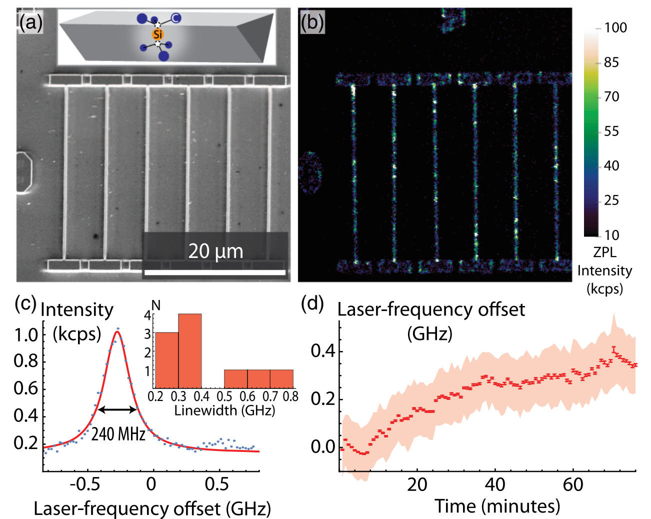

FIG. 3. SiV^- centers in nanostructures. (a) Scanning electron micrograph of six nanobeam waveguides. Inset: schematic of a triangular diamond nanobeam containing an SiV^- center. (b) Spatial map of ZPL fluorescence collected by scanning confocal microscopy with off-resonant excitation. Multiple SiV^- centers are visible in each waveguide. (c) Linewidth of representative implanted SiV^- inside a nanowaveguide measured by PLE spectroscopy (blue points, data; red line, Lorentzian fit). Inset: histogram of emitter linewidths in nanostructures. Most emitters have linewidths within a factor of 4 of the lifetime limit. (d) Spectral diffusion of the emitter measured in part (c). The total spectral diffusion is under 400 MHz even after more than an hour of continuous measurement. This diffusion is quantified by measuring the drift of the fitted center frequency of resonance fluorescence scans as a function of time. Error bars are statistical error on the fitted center position. The lighter outline is the FWHM of the fitted Lorentzian at each time point.

fluorescence image of the final structures [Fig. 3(b)]. Photon correlation measurements (Appendix B) verify our ability to create and image single SiV^- centers.

To characterize the optical coherence properties of SiV^- centers in nanostructures, we again perform PLE spectroscopy. SiV^- centers in nanostructures have narrow transitions with a FWHM of $\Gamma_n/2\pi = 410 \pm 160$ MHz [the mean and standard deviation for $N = 10$ emitters; see the Fig. 3(c) inset for the linewidth histogram], only a factor of 4.4 greater than the lifetime-limited linewidth $\gamma/2\pi = 94$ MHz. The linewidths measured in nanostructures are comparable to those measured in bulk (unstructured) diamond ($\Gamma_b/2\pi = 320 \pm 180$ MHz). The ratios Γ_n/γ and Γ_b/γ are much lower than the values for NV^- centers, where the current state of the art for typical implanted NV^- centers in nanostructures [9] and in bulk [31] is $\Gamma_n/\gamma \gtrsim 100$–200 and $\Gamma_b/\gamma \gtrsim 10$ ($\gamma/2\pi = 13$ MHz for NV^- centers).

It is possible for the lifetime in nanostructures to be longer than the lifetime in the bulk since the local photonic density of states is generally reduced inside such a structure [46,47]. This potential change in lifetime would change the lifetime-limited linewidth and can also provide indirect evidence of the SiV^- quantum efficiency. To probe this effect, we measured the lifetime of nine SiV^- centers. The lifetime measured in the nanobeam waveguides ($\tau = 1.69 \pm 0.14$ ns, $N = 5$) was not significantly different from the lifetime measured in the bulklike anchors ($\tau = 1.75 \pm 0.08$ ns, $N = 4$). Both values are in good agreement with the literature [24,29].

By extracting the center frequency of each individual scan, we also determine the rate of fluctuation of the ZPL frequency and therefore quantify spectral diffusion [Fig. 3(d)]. Optical transition frequencies in SiV^- centers are stable throughout the course of our experiment, with spectral diffusion on the order of the lifetime-limited linewidth even after more than an hour. Characterizing the inhomogeneous distribution of SiV^- centers in nanostructures is challenging because off-resonant excitation leads to strong background fluorescence, making exhaustive identification of all SiV^- centers in a given region difficult. Nevertheless, it is easy to find multiple SiV^- centers in nanostructures at nearly the same resonance frequency: to find the above ten emitters, we scanned the laser frequency over only a 20-GHz range.

The residual broadening of the optical transition can result from a combination of second-order Stark shifts and phonon-induced broadening. The presence of a strong static electric field would result in an induced dipole that linearly couples to charge fluctuations, accounting for the slow diffusion. Finally, we expect that up to 50 MHz of additional broadening could arise from the hyperfine interaction [48] present due to our choice of ^{29}Si ions. Determining the precise mechanisms limiting SiV^- linewidths is an important topic of future study.

To conclude, we have presented optical emission from implanted SiV^- centers with a narrow inhomogeneous distribution of SiV^- optical transition wavelengths and nearly lifetime-limited optical linewidths. These properties persist after nanofabrication, making the SiV^- center uniquely suited for integration into quantum nanophotonic devices [49,50]. Recent advances in diamond fabrication technology [30,51,52] suggest the tantalizing possibility of scalably integrating these high-quality implanted SiV^- centers into nanowire single-photon sources [46] or nanocavities [53,54]. Furthermore, combining our processing procedure with targeted implantation of silicon using a focused ion beam [22] either before or after fabrication [55] could significantly improve photonic device yields and reproducibility by deterministically positioning individual SiV^- centers in all three dimensions. Our work, combined with the promise of these future advances, could make the SiV^- center a workhorse in solid-state quantum optics.

ACKNOWLEDGMENTS

We thank D. J. Twitchen and M. Markham from Element Six Inc. for providing the electronic-grade diamond samples, A. Sushkov and S. Meesala for help with annealing, and N. P. de Leon and K. De Greve for help with etching and sample processing. We also thank Y. Chu, B. J. Shields, K. D. Jahnke, L. J. Rogers, and F. Jelezko for discussions and valuable insight. M. L. Goldman and C. T. Nguyen helped develop some of the software used in the experiment. M. K. Bhaskar contributed to figure design. Financial support was provided by the NSF, the Center for Ultracold Atoms, the Air Force Office of Scientific Research MURI "Multifunctional Light-Matter Interfaces based on Neutral Atoms & Solids," the DARPA QuINESS program, and the ARL. R. E. was supported in part by the NSF Graduate Research Fellowship Program. This work was performed in part at the Center for Nanoscale Systems (CNS) of Harvard University, which is supported under NSF Grant No. ECS-0335765.

R. E. E. and A. S. contributed equally to this work.

APPENDIX A: EXPERIMENTAL SETUP

The experiments are carried out using home-built scanning confocal microscopes as illustrated in Fig. 4. The three lasers used for excitation (520-nm and 700-nm diode lasers used for off-resonant excitation, 737-nm external-cavity diode laser used for resonant excitation) are combined using dichroic beam splitters. A 760-nm long-pass dichroic beam splitter separates the PSB fluorescence from the rest of the optical channels. An additional bandpass filter (740 ± 13 nm) is used on the ZPL channel. Single photons are detected using single-photon counting modules (Picoquant τ-SPAD and Excelitas SPCM-NIR). The cryogenic measurements are performed in 4-K helium-flow cryostats. We used a 0.95 NA microscope objective (Nikon CFI LU Plan Apo Epi 100×) in all experiments. During the

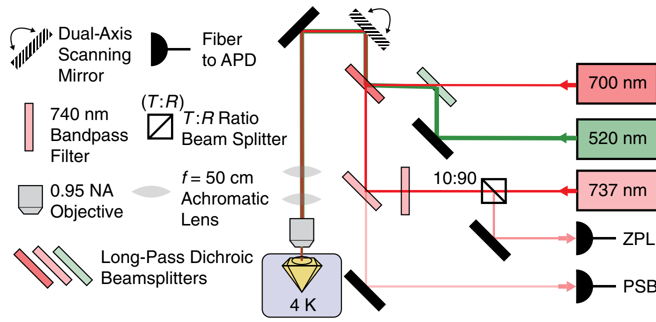

FIG. 4. Confocal microscope design. The 520-nm and 700-nm lasers are used to excite the SiV^- off resonantly. The 737-nm external-cavity diode laser is used to excite the SiV^- resonantly. Optical fibers are used to collect the SiV^- fluorescence and transmit it to avalanche photodiodes (APDs) for detection. Collection can be performed either on the ZPL (if the excitation is off resonance) or the PSB (in either excitation scheme).

cryogenic measurements, the objective is inside the vacuum chamber and the sample is clamped with an indium foil spacer to the cold finger of the cryostat. During the PLE measurements, the 520-nm laser is pulsed at a ∼5% duty cycle to stabilize the charge state of the SiV^- center [9,31]. The detectors are gated off during these pulses.

APPENDIX B: FLUORESCENCE AUTOCORRELATION MEASUREMENTS

To verify our ability to create single SiV^- centers, we perform fluorescence autocorrelation measurements on SiV^- centers inside diamond nanobeams. We perform this measurement by exciting the SiV^- centers off resonantly as described above and splitting the emission between two detectors in a Hanbury-Brown–Twiss configuration. The relative arrival times of the photons on the two detectors are recorded using fast acquisition electronics (PicoQuant HydraHarp 400) with a resolution better than 128 ps. In this experiment, our total average photon count rate from this SiV^- is 9×10^4 counts per second.

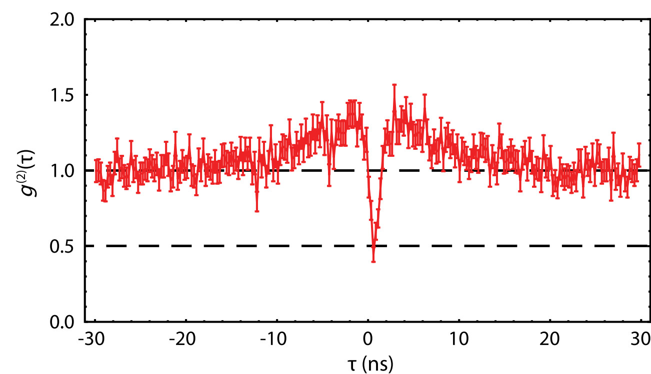

FIG. 5. Fluorescence autocorrelation measurement of a SiV^- center inside a diamond nanobeam as described in the text. Error bars are estimated assuming the noise on the number of detected photons follows a Poisson distribution (shot noise). The extent of the dip at $\tau = 0$ is limited by finite detector bandwidth: we measure $g^{(2)}(0) = 0.45$; deconvolving the detector response yields $g^{(2)}(0) = 0.15$.

The relative photon detection times $g^{(2)}(\tau)$ [normalized by defining $g^{(2)}(\infty) = 1$] from a representative SiV^- are displayed in Fig. 5. A value of $g^{(2)}(0) < 0.5$ would confirm that we are measuring emitters producing single photons. Finite jitter on our detectors of around 350 ps causes the measured arrival times of our photons to be convolved with the detector response, hence limiting the sharpness and minimum value of our dip. Fitting the data (including the detector response) using previously reported methods [14] gives a value $g^{(2)}(0) = 0.45$. Deconvolving the detector response gives a value $g^{(2)}(0) = 0.15$, indicating that the extent of our $g^{(2)}(0)$ dip is limited primarily by detector response as expected.

[1] J. L. O'Brien, A. Furusawa, and J. Vučković, Photonic quantum technologies, Nat. Photonics **3**, 687 (2009).
[2] P. Lodahl, S. Mahmoodian, and S. Stobbe, Interfacing single photons and single quantum dots with photonic nanostructures, Rev. Mod. Phys. **87**, 347 (2015).
[3] M. W. Doherty, N. B. Manson, P. Delaney, F. Jelezko, J. Wrachtrup, and L. C. Hollenberg, The nitrogen-vacancy colour centre in diamond, Phys. Rep. **528**, 1 (2013).
[4] H. Bernien, B. Hensen, W. Pfaff, G. Koolstra, M. S. Blok, L. Robledo, T. H. Taminiau, M. Markham, D. J. Twitchen, L. Childress, and R. Hanson, Heralded entanglement between solid-state qubits separated by three metres, Nature (London) **497**, 86 (2013).
[5] B. Hensen *et al.*, Loophole-free Bell inequality violation using electron spins separated by 1.3 kilometres, Nature (London) **526**, 682 (2015).
[6] W. Pfaff *et al.*, Unconditional quantum teleportation between distant solid-state quantum bits, Science **345**, 532 (2014).
[7] P. Tamarat *et al.*, Stark Shift Control of Single Optical Centers in Diamond, Phys. Rev. Lett. **97**, 083002 (2006).
[8] P. Siyushev, H. Pinto, M. Vörös, A. Gali, F. Jelezko, and J. Wrachtrup, Optically Controlled Switching of the Charge State of a Single Nitrogen-Vacancy Center in Diamond at Cryogenic Temperatures, Phys. Rev. Lett. **110**, 167402 (2013).
[9] A. Faraon, C. Santori, Z. Huang, V. M. Acosta, and R. G. Beausoleil, Coupling of Nitrogen-Vacancy Centers to Photonic Crystal Cavities in Monocrystalline Diamond, Phys. Rev. Lett. **109**, 033604 (2012).
[10] E. Neu, D. Steinmetz, J. Riedrich-Möller, S. Gsell, M. Fischer, M. Schreck, and C. Becher, Single photon emission from silicon-vacancy colour centres in chemical vapour deposition nano-diamonds on iridium, New J. Phys. **13**, 025012 (2011).
[11] L. J. Rogers *et al.*, Multiple intrinsically identical single-photon emitters in the solid state, Nat. Commun. **5**, 4739 (2014).
[12] H. Sternschulte, K. Thonke, R. Sauer, P. C. Münzinger, and P. Michler, 1.681-eV luminescence center in

chemical-vapor-deposited homoepitaxial diamond films, Phys. Rev. B **50**, 14554 (1994).
[13] C. Hepp *et al.*, Electronic Structure of the Silicon Vacancy Color Center in Diamond, Phys. Rev. Lett. **112**, 036405 (2014).
[14] A. Sipahigil, K. D. Jahnke, L. J. Rogers, T. Teraji, J. Isoya, A. S. Zibrov, F. Jelezko, and M. D. Lukin, Indistinguishable Photons from Separated Silicon-Vacancy Centers in Diamond, Phys. Rev. Lett. **113**, 113602 (2014).
[15] T. Müller, C. Hepp, B. Pingault, E. Neu, S. Gsell, M. Schreck, H. Sternschulte, D. Steinmüller-Nethl, C. Becher, and M. Atatüre, Optical signatures of silicon-vacancy spins in diamond, Nat. Commun. **5**, 3328 (2014).
[16] C. Lo, Natural colorless type IaB diamond with silicon-vacancy defect center, Gems Gemol. **L**, 293 (2014).
[17] A. M. Edmonds, M. E. Newton, P. M. Martineau, D. J. Twitchen, and S. D. Williams, Electron paramagnetic resonance studies of silicon-related defects in diamond, Phys. Rev. B **77**, 245205 (2008).
[18] U. F. S. D'Haenens-Johansson, A. M. Edmonds, B. L. Green, M. E. Newton, G. Davies, P. M. Martineau, R. U. A. Khan, and D. J. Twitchen, Optical properties of the neutral silicon split-vacancy center in diamond, Phys. Rev. B **84**, 245208 (2011).
[19] E. Neu, C. Hepp, M. Hauschild, S. Gsell, M. Fischer, H. Sternschulte, D. Steinmüller-Nethl, M. Schreck, and C. Becher, Low-temperature investigations of single silicon vacancy colour centres in diamond, New J. Phys. **15**, 043005 (2013).
[20] C. D. Clark, H. Kanda, I. Kiflawi, and G. Sittas, Silicon defects in diamond, Phys. Rev. B **51**, 16681 (1995).
[21] J. L. Zhang, H. Ishiwata, T. M. Babinec, M. Radulaski, K. Mller, K. G. Lagoudakis, C. Dory, J. Dahl, R. Edgington, V. Soulire, G. Ferro, A. A. Fokin, P. R. Schreiner, Z.-X. Shen, N. A. Melosh, and J. Vučković, Hybrid group IV nano-photonic structures incorporating diamond silicon-vacancy color centers, Nano Lett. **16**, 212 (2016).
[22] S. Tamura *et al.*, Array of bright silicon-vacancy centers in diamond fabricated by low-energy focused ion beam implantation, Appl. Phys. Express **7**, 115201 (2014).
[23] C. Wang, C. Kurtsiefer, H. Weinfurter, and B. Burchard, Single photon emission from SiV centres in diamond produced by ion implantation, J. Phys. B **39**, 37 (2006).
[24] B. Pingault, J. N. Becker, C. H. H. Schulte, C. Arend, C. Hepp, T. Godde, A. I. Tartakovskii, M. Markham, C. Becher, and M. Atatüre, All-Optical Formation of Coherent Dark States of Silicon-Vacancy Spins in Diamond, Phys. Rev. Lett. **113**, 263601 (2014).
[25] I. Aharonovich, S. Castelletto, D. Simpson, C. Su, A. Greentree, and S. Prawer, Diamond-based single-photon emitters, Rep. Prog. Phys. **74**, 076501 (2011).
[26] J. P. Goss, R. Jones, S. J. Breuer, P. R. Briddon, and S. Öberg, The Twelve-Line 1.682 eV Luminescence Center in Diamond and the Vacancy-Silicon Complex, Phys. Rev. Lett. **77**, 3041 (1996).
[27] L. J. Rogers *et al.*, Electronic structure of the negatively charged silicon-vacancy center in diamond, Phys. Rev. B **89**, 235101 (2014).
[28] A. Gali and J. R. Maze, *Ab initio* study of the split silicon-vacancy defect in diamond: Electronic structure and related properties, Phys. Rev. B **88**, 235205 (2013).
[29] K. D. Jahnke, A. Sipahigil, J. M. Binder, M. W. Doherty, M. Metsch, L. J. Rogers, N. B. Manson, M. D. Lukin, and F. Jelezko, Electron-phonon processes of the silicon-vacancy centre in diamond, New J. Phys. **17**, 043011 (2015).
[30] M. J. Burek, N. P. de Leon, B. J. Shields, B. J. Hausmann, Y. Chu, Q. Quan, A. S. Zibrov, H. Park, M. D. Lukin, and M. Lončar, Free-standing mechanical and photonic nanostructures in single-crystal diamond, Nano Lett. **12**, 6084 (2012).
[31] Y. Chu, N. P. de Leon, B. J. Shields, B. Hausmann, R. Evans, E. Togan, M. J. Burek, M. Markham, A. Stacey, A. S. Zibrov, A. Yacoby, D. J. Twitchen, M. Lončar, H. Park, P. Maletinsky, and M. D. Lukin, Coherent optical transitions in implanted nitrogen vacancy centers, Nano Lett. **14**, 1982 (2014).
[32] J. F. Ziegler, M. D. Ziegler, and J. P. Biersack, SRIM—The stopping and range of ions in matter (2010), Nucl. Instrum. Methods Phys. Res., Sect. B **268**, 1818 (2010).
[33] M. Hauf *et al.*, Chemical control of the charge state of nitrogen-vacancy centers in diamond, Phys. Rev. B **83**, 081304 (2011).
[34] G. Davies, S. C. Lawson, A. T. Collins, A. Mainwood, and S. J. Sharp, Vacancy-related centers in diamond, Phys. Rev. B **46**, 13157 (1992).
[35] P. Deák, B. Aradi, M. Kaviani, T. Frauenheim, and A. Gali, Formation of NV centers in diamond: A theoretical study based on calculated transitions and migration of nitrogen and vacancy related defects, Phys. Rev. B **89**, 075203 (2014).
[36] A. M. Zaitsev, *Optical Properties of Diamond: A Data Handbook* (Springer-Verlag Berlin Heidelberg, Berlin, Heidelberg, 2001).
[37] V. Acosta *et al.*, Diamonds with a high density of nitrogen-vacancy centers for magnetometry applications, Phys. Rev. B **80**, 115202 (2009).
[38] T. Yamamoto *et al.*, Extending spin coherence times of diamond qubits by high-temperature annealing, Phys. Rev. B **88**, 075206 (2013).
[39] C. D. Clark and C. Dickerson, The 1.681 eV centre in polycrystalline diamond, Surf. Coat. Technol. **47**, 336 (1991).
[40] S. Pezzagna, B. Naydenov, F. Jelezko, J. Wrachtrup, and J. Meijer, Creation efficiency of nitrogen-vacancy centres in diamond, New J. Phys. **12**, 065017 (2010).
[41] J. Orwa *et al.*, Engineering of nitrogen-vacancy color centers in high purity diamond by ion implantation and annealing, J. Appl. Phys. **109**, 083530 (2011).
[42] T. D. Ladd, F. Jelezko, R. Laflamme, Y. Nakamura, C. Monroe, and J. L. O'Brien, Quantum computers, Nature (London) **464**, 45 (2010).
[43] K. J. Vahala, Optical microcavities, Nature (London) **424**, 839 (2003).
[44] Y. Li, P. C. Humphreys, G. J. Mendoza, and S. C. Benjamin, Resource Costs for Fault-Tolerant Linear Optical Quantum Computing, Phys. Rev. X **5**, 041007 (2015).
[45] B. J. Hausmann *et al.*, Coupling of NV centers to photonic crystal nanobeams in diamond, Nano Lett. **13**, 5791 (2013).

[46] T. M. Babinec, B. J. Hausmann, M. Khan, Y. Zhang, J. R. Maze, P. R. Hemmer, and M. Lončar, A diamond nanowire single-photon source, Nat. Nanotechnol. **5**, 195 (2010).

[47] Y. Chu and M. D. Lukin, Quantum optics with nitrogen-vacancy centers in diamond, arXiv:1504.05990.

[48] L. J. Rogers *et al.*, All-Optical Initialization, Readout, and Coherent Preparation of Single Silicon-Vacancy Spins in Diamond, Phys. Rev. Lett. **113**, 263602 (2014).

[49] I. Aharonovich, A. D. Greentree, and S. Prawer, Diamond photonics, Nat. Photonics **5**, 397 (2011).

[50] B. J. Hausmann *et al.*, Integrated diamond networks for quantum nanophotonics, Nano Lett. **12**, 1578 (2012).

[51] J. Riedrich-Möller *et al.*, One-and two-dimensional photonic crystal microcavities in single crystal diamond, Nat. Nanotechnol. **7**, 69 (2012).

[52] M. J. Burek, Y. Chu, M. S. Liddy, P. Patel, J. Rochman, S. Meesala, W. Hong, Q. Quan, M. D. Lukin, and M. Lončar, High quality-factor optical nanocavities in bulk single-crystal diamond, Nat. Commun. **5**, 5718 (2014).

[53] J. C. Lee, I. Aharonovich, A. P. Magyar, F. Rol, and E. L. Hu, Coupling of silicon-vacancy centers to a single crystal diamond cavity, Opt. Express **20**, 8891 (2012).

[54] J. Riedrich-Möller, C. Arend, C. Pauly, F. Mucklich, M. Fischer, S. Gsell, M. Schreck, and C. Becher, Deterministic coupling of a single silicon-vacancy color center to a photonic crystal cavity in diamond, Nano Lett. **14**, 5281 (2014).

[55] A. Sipahigil, R. E. Evans, D. D. Sukachev, M. J. Burek, C. T. Nguyen, J. Borregaard, M. K. Bhaskar, J. L. Pacheco, H. Atikian, R. M. Camacho, F. Jelezko, E. Bielejec, H. Park, M. Lončar, and M. D. Lukin (unpublished).